Final published version is available at ScienceDirect: http://dx.doi.org/10.1016/j.spmi.2017.03.053

Texture of Al Films for Wafer-Level Thermocompression Bonding

N. Malik[a, b, *], V. Venkatachalapathy[a], W. Dall[c], K. Schjølberg-Henriksen[b], E. Poppe[b], M. M. Visser Taklo[b], T. G. Finstad[a]

[a]*Centre for Materials Science and Nanotechnology, University of Oslo, PO Box 1032 Blindern, N-0315 Oslo, Norway*

[b]*SINTEF ICT, Department of Microsystems and Nanotechnology, PO Box 124 Blindern, N-0314 Oslo, Norway*

[c]*SINTEF Materials and Chemistry, Department of Industrial Process Technology, PO Box 4760 Sluppen, 7465 Trondheim, Norway*

[d]*SINTEF ICT, Department of Instrumentation, PO Box 124 Blindern, N-0314 Oslo, Norway*

Keywords: Aluminium, Thin film, Wafer bonding, X-ray diffraction (XRD), Electron backscatter diffraction (EBSD)

Abstract

Properties of aluminum (Al) thin films for thermocompression bonding have been studied in terms of surface roughness (SR), grain size, and grain orientation by atomic force microscope (AFM), scanning electron microscope (SEM), X-ray diffraction (XRD) and electron backscatter diffraction (EBSD). Al films were sputter deposited directly on Si and (wet) thermally oxidized Si wafers, respectively. The resulting Si/Al and Si/SiO_2/Al sample types were compared after annealing at temperatures of 300, 400, and 550 °C in vacuum. The Si/SiO_2/Al film samples showed higher surface roughness than the Si/Al samples. The annealed samples had a large number of hillocks for both sample types. The as-deposited films had (111) preferred orientation. However XRD analysis and EBSD analysis also revealed (111), (100) and (110) oriented Al grains for the Si/SiO_2/Al samples while only (111) oriented grains for the Si /Al samples. The Si/SiO_2/Al samples had a conical <111> texture with a semi-apex angle about 6.3 degrees. A similar conical texture with a semi-apex angle of 3.2 degrees was observed for Si/Al samples after annealing at 550 °C. The Si/Al samples had a <111> fibrous texture in the as-deposited state. The observed evolution of the grain structure with annealing temperature is discussed in terms of native oxide, surface roughness, diffusivity and grain orientation dependent mechanical properties in order to shine light on previously observed differences in Al-Al thermocompression wafer-level bonding with Si/SiO_2/Al and Si/Al wafers.

[*]Corresponding author.

E-mail address: nishantmalik1987@gmail.com

1. Introduction

Micro electromechanical systems (MEMS) such as resonators, gyroscopes, accelerators etc. contain movable structures which not only need protection against mechanical damage but often require vacuum environment in order to function. The packaging of MEMS devices accounts for >50 % of the manufacturing cost of the device [1]. Wafer level packaging (WLP) provides a cost effective way of sealing MEMS devices in large volume production [2]. Wafer bonding is the most commonly used wafer level packaging for MEMS.

Among the wide range of wafer bonding techniques, metal thermocompression bonding has recently attracted increased interest [3]. Metal thermocompression bonding is a method for joining two metal surfaces together by application of temperature and pressure. Metal seals are hermetic for a longer time compared to non-metal seals of the same seal width [4]. Therefore, metals enable a reduction of seal width, thereby reducing the device size. Additionally, metals can provide electrical interconnections as well as mechanical stability in the same fabrication step. Metals such as Au [5], Cu [6] and Al [7-10] have been demonstrated as bonding layers between two Si wafers. STMicroelectronics reported a reduction of 57 % in size of their accelerometers by replacing glass-frit bonding by Au-Au thermocompression bonding [11]. Seal rings as narrow as 10 µm have been investigated by Analog Devices using Al-Al thermocompression bonding [12].

Among a range of metals, Al is highly attractive as it can be easily integrated in a CMOS process. Successful Al-Al thermocompression bonding has been reported in the literature. However, the influence of the Al film morphology and texture on the films bonding properties has not been reported. A systematic study of varying bond force (9, 14 and 18 kN) and Cu impurity content (0–4 %) in Al was presented by Yun et al. [10]. The bonding temperature was kept constant at 450 °C. Increasing the bond force resulted in an increase in the yield and the shear strength of the bonds. Pure Al gave the highest yield, while Al with 4 % Cu gave the highest shear strength. Dragoi et al. [7] studied the effect of varying bonding temperature (400–550 °C) at 50 °C intervals, varying the bonding time (1 and 4 h) and varying the bonding environments (N_2 and H_2:Ar) . Different bonding environment and time did not affect the bond quality, while a trend of increasing interfacial adhesion energy with increasing bonding temperature was observed. A threshold was reported in interfacial adhesion energy measurements between bonds performed at 450 °C and 500 °C.

We have reported Al-Al thermocompression bonding at a range of bonding temperatures, forces and times in our earlier works [8, 9, 13]. For reduction of the bonding temperature, it was beneficial to sputter deposit the bonding Al film onto a thermally oxidized Si surface compared to depositing directly on a Si surface [13]. In order to understand the effect this SiO_2 layer had on the Al-Al bonding, we have here conducted systematic morphological studies of Al thin films deposited on Si and thermally oxidized Si wafers respectively, and we report on these studies in this work. The films were annealed at various temperatures. The objective was to investigate

whether differences in the Al film morphology on these two kinds of substrates could be related to the observed differences in the previously observed bonding results.

Al films have been utilized as conducting paths in microelectronics where they have been deposited on Si and on Si/SiO_2. This could indicate that the morphology of the Al films in our previous bonding experiments could be found from previous measurements reported in the literature. However, despite the long history of literature on Al films [14-16], there exist fewer detailed studies than expected. There is also less literature on pure Al films than on Al films with additions of Cu and/or Si which have been more commonly used in microelectronics [17, 18]. A (111) preferred orientation for Al thin films has been reported [16], which is typical for fcc metals. Multiple other orientations have also been observed as well as epitaxial relations between the Al film and the Si substrate [19-21]. Earlier results show that the Al thin film texture depends upon several parameters in addition to the type of substrate and deposition method used. It depends strongly on residual gas pressure during deposition [22]. Further, the Al thin film texture depends strongly on the energy of the deposited atoms and on the substrate temperature [23]. For sputter-based deposition, the energy of the deposited atoms is influenced by the applied power, the pressure, and it may also depend upon the design of the sputter system [24, 25]. We therefor set out to investigate the morphology of Al films sputter deposited with the same parameters in the same system as was used in our previous bonding experiments. With the wide use of Al films, the obtained results may be of interest to a wider community than the wafer bonding community.

2. Experimental

Eight single side polished (100) silicon wafers of diameter 150 mm and thickness 625 µm, were used in the experiment. Four of the wafers were subjected to a wet thermal oxidation process to form a nominal SiO_2 layer thickness of 150 nm. All eight wafers were sputter deposited with 1 µm thick layer of pure Al (99.999 %) on the polished side. All wafers were subjected to standard RCA cleaning steps before oxidation and Al deposition. The Al films were deposited in a DC magnetron sputtering system, operated at 5 kW using Ar gas at a chamber pressure of 10 mT. The base pressure of the sputtering chamber before feeding of Ar gas was 3×10^{-7} Torr. The Al target diameter was 8 inch. The substrate was at room temperature before the deposition process and the substrate temperature at the end of the sputtering process was found to be ~120 °C. The deposition rate was about 0.36 µm/min. Prior to deposition, an additional *in situ* back-sputter etch was included for all wafers. For the wafers without a thermal SiO_2 this should completely remove the native oxide.

Three wafers from each type (Si /Al and Si/SiO_2/Al) were annealed in an EVG®510 bonder at a temperature of either 300, 400 or 550 °C for a duration of 1 h in vacuum, without applying any compressive force on the samples. The pressure in the chamber was 6 mT before the heating was turned on. The heating and cooling rates were 45 °C/min and 10 °C/min, respectively. The as-deposited Si/Al and Si/SiO_2/Al samples have been labeled SiRT and OxRT respectively. The

post-annealed samples have been labeled with their annealing temperatures as Si300, Si400, Si550 or Ox300, Ox400, Ox550 for Si/Al and Si/SiO_2/Al samples, respectively.

The surface roughness (SR) of all samples was measured by a Dimension 3100 (Veeco instruments Inc.) atomic force microscope (AFM) operated in tapping mode. The SR was estimated as an average of 3 to 5 AFM raster scans performed in an area of 1 or 5 μm^2. The software SPIP™ by Image Metrology [26] was used for the analysis of the data extracted from the AFM. Free-standing hillocks on the Al surface were excluded from the SR estimation from the AFM data. The distribution of hillocks on the surface of Al films annealed at various temperatures was analyzed by a scanning electron microscope (SEM, FEI Quanta FEG 600) in an area of 52×52 μm^2 for all samples. The number of hillocks and coverage by hillocks i.e. the percentage of area covered by hillocks in the investigated area was estimated by the software SPIP™.

X-ray diffraction (XRD) analyses of the Al films were performed (Bruker AXS D8 Discover, Cu $K\alpha_1$ X-rays) to study the texture (distribution of crystallographic orientations) of the films. The X-ray beam size was 16×0.2 mm. We use the following notation for the angles of the system: 2θ: angle between X-ray source and detector; ω: sample tilt angle with axis normal to the plane of the X-ray source and the detector; Φ: in-plane sample rotation. All rotation angles were assumed to cross at the same point and were independent. A normal θ-2θ scan (locked-couple mode) was performed to determine the preferred crystal orientation of the film. A set of rocking curve (ω-scan) measurements at a series of Φ-angles were performed in order to study texture of the preferred orientations. In the ω-scan measurements, the angle between the source and detector directions was fixed at $2\theta_B$, corresponding to the Bragg conditions for the crystallographic plane of interest (here the {111} planes). We also defined the zero point for ω from the Bragg condition, and $\omega = \Omega - \theta_B$, where Ω is the angle between the film plane and the X-rays from the source. The ω-scan measurements were done for a set of in-plane sample rotation angles, Φ, covering 360° and being separated by 15° of rotation. These measurements provided the orientation distribution for the (111) oriented grains, which will be referred to as the (111) grain distribution (GD). On the ω-scan curve the amplitude is a measure of the amount of Al in grains that had their [111] direction in a direction given by ω (polar angle) and Φ (azimuthal angle). The tilt of the Al [111] direction with respect to the surface normal for each grain contributing to a point on the curve is given by ω. The ω-value of the maximum of the ω-scan curve gave the tilt angle of the [111] axis of the most prominent orientation of Al grains with respect to the surface normal for a particular Φ. The Φ-value that gave the maximum X-ray intensity in the rocking curve measurements was then used to perform a locked-coupled mode scan which was used to determine the (111) interplanar spacing in the contributing grains. The Scherrer formula [27] was applied to the width of the diffraction peaks obtained by this locked-coupled scan to yield a lower limit for an estimate of the grain size. To look into the surface grain orientations, misorientations among grains and grain size distribution, electron backscattering diffraction (EBSD) data was collected on a Hitachi SU-6600 SEM equipped with

a Nordif ultra-fast EBSD detector controlled by Nordif Data Collection software [28]. Results from the data collection were later indexed and analyzed with the EDAX TSL-OIM Software suit v.7.2 [29]. Since the Si substrate pieces were cut with edges and surface normal close to <100> directions, the standard inverse pole figures (with respect to instrument standard directions) could be interpreted directly with respect to the Si crystallographic directions.

3. Results

3.1 Summary of our previous bonding experiment results

The dicing yield results of bonded laminates from our earlier work are shown in Fig. 1 [13]. The dicing yield is a qualitative measure of the quality of the bonding. One can clearly see from Fig. 1 that the dicing yield for all laminates where the bonding Al was deposited on SiO_2 ($Si/SiO_2/Al$) was above 95 % for bonding temperatures down to 300 °C. No bonding was observed for Si/Al based laminates bonded at temperatures lower than 400 °C. The laminates without a SiO_2 layer (Si/Al), had a dicing yield above 95 % only for bonding temperatures ≥ 450 °C. The yield of the Si/Al laminate bonded at 400 °C was below 34 %, thus there was a clear difference in the bonding quality at this temperature for laminates with and without SiO_2.

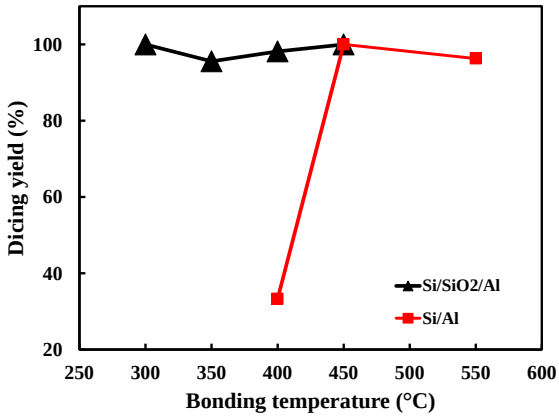

Fig. 1. Dicing yield of bonded laminates of two different structures bonded with identical parameters at different temperatures. The figure summarizes an important trend for previous results: Al films deposited on a thermal oxide ($Si/SiO_2/Al$) could be wafer bonded with a dicing yield above 95 %, whereas it was not possible to bond Al films deposited on Si (Si/Al) below 400 °C and the dicing yield was low at 400 °C. All bondings were done for 60 min with an applied force of 36 kN [13].

3.2. Surface roughness

Fig. 2 shows the SR values (RMS) of all the Si/Al and the $Si/SiO_2/Al$ films. The SR of both the Si/Al and $Si/SiO_2/Al$ films increased with increasing annealing temperature. The SR of the Si/Al films increased from 1.90 nm to 5.54 nm, while the SR of the $Si/SiO_2/Al$ films increased from 3.28 nm to 8.04 nm as the annealing temperature was increased from RT to 550 °C. The surface roughness of the $Si/SiO_2/Al$ films was higher than that of the Si/Al films for all temperatures. The SEM images of the Al surfaces for both the Si/Al and the $Si/SiO_2/Al$ films are

shown in Fig. 3. No hillocks were observed for the as-deposited samples. After annealing, the density of hillocks was higher on the Si/SiO_2/Al than on the Si/Al surface. For Si- and Ox-samples, an increase in the density of hillocks and in the coverage by hillocks on surfaces was observed with increasing annealing temperature up to 400 °C. Further increasing the annealing temperature from 400 to 550 °C caused a decrease in the density of hillocks and the area covered by hillocks (which was almost the same for both samples). The hillocks varied largely in height; the AFM scans indicated the height being typically in the range 50-200 nm.

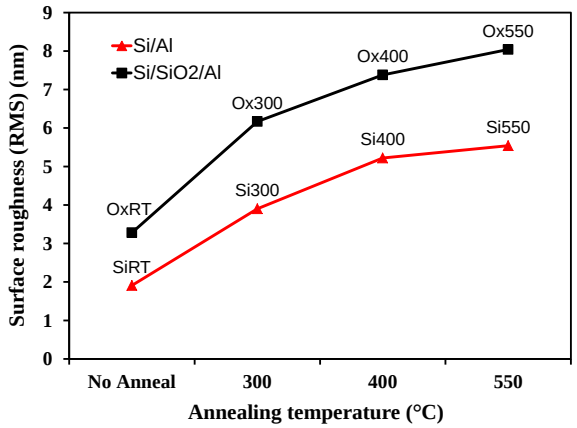

Fig. 2. Surface roughness determined by AFM of as-deposited and annealed 1 µm thick Al films sputtered deposited on Si and on oxidized Si having a 150 nm thick SiO_2 layer. The samples were annealed at temperatures of 300, 400 and 550 °C for 1 h in vacuum.

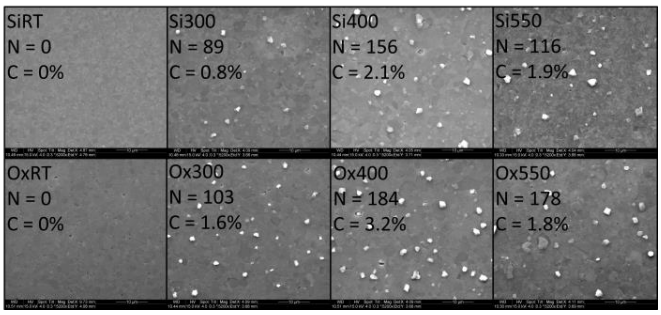

Fig. 3. The SEM image of the Al surface annealed at various temperatures. The Al is deposited directly on Si and on top of an oxidized Si wafer. The wafers were annealed at 300, 400 and 550 °C for 1 h in vacuum. Here, N represents the number of hillocks observed on the Al surface and C represents the coverage by hillocks i.e. the percentage of area covered by hillocks in the image.

3.3. XRD results

3.3.1. Preferential orientations

The θ-2θ scan spectra of the as-deposited Si/Al and Si/SiO_2/Al films are shown in Fig. 4. Fig. 4(A) and (B) represent XRD results of sample SiRT and OxRT, respectively, in the 2θ range of 35–80°. The peak at 69.1° corresponds to diffraction of the (400) lattice planes in Si. The highest peak intensity obtained from the Al film was at 38.4° for both samples, indicating that the Al

(111) lattice plane was preferentially parallel to the substrate plane. However, in sample OxRT, other non-(111) low intensity 2θ peaks at 44.7°, 65° and 78.2° corresponding to the (200), (220) and (311) lattice planes in Al were observed in addition to the peak at 38.4°. This indicates that the Si/SiO_2/Al film contained grains of multiple orientations, but with a (111) preferred orientation. The peak observed at 61.7° corresponds to the Kβ Si (400) peak. The post-annealed Si/Al films (Si300, Si400 and Si550) exhibited XRD features similar to the SiRT sample. The post-annealed samples Ox300 and Ox400 had the same features as the OxRT sample. In contrast, only the (111) peak was observed in the Ox550 sample. The inset in Fig. 4 shows the *θ-2θ* scan of sample Ox550, where only a peak at 38.4° was observed. This peak corresponds to the (111) lattice plane of Al. No peak at 44.7° was observed for the Al (220) lattice plane in sample Ox550.

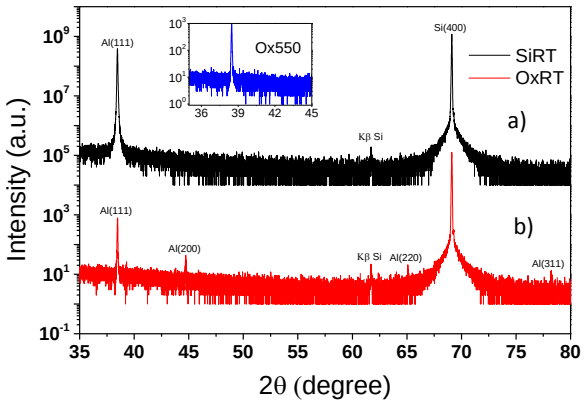

Fig. 4. θ-2θ X-ray diffraction (XRD) scans of 1 µm thick Al films deposited (a) on Si (SiRT) and (b) on oxidized Si (OxRT) having a 150 nm thick SiO2 layer. The inset shows the θ-2θ scan of Al film with SiO2 layer underneath and annealed at 550 °C for 1h (Ox550).

Table 1 presents the peak ratios I(220)/I(111) for the various Si/SiO_2/Al samples. The I(220)/I(111) ratio decreased with increasing annealing temperature for the Si/SiO_2/Al samples, indicating the tendency towards (111) preferential orientation with higher annealing temperatures.

T (°C)	Intensity ratio (I) (220)/(111)		Strain	
	Si/Al	Si/SiO_2/Al	Si/Al	Si/SiO_2/Al
No Anneal	–	0.054	0.0011	0.0003
300	–	0.046	0.0009	0.0011
400	–	0.033	0.0007	0.0005
550	–	–	0.0009	0.0010

Table 1. Overview of intensity ratios from 2*θ* locked-couple XRD scan for un-annealed and annealed wafers at temperatures of 300, 400 and 550 °C for 1 hour with Si or SiO_2 underneath Al film. Strain as calculated from *ω*-2*θ* XRD scan for the Φ-angles giving two maximum intensity peaks as seen in rocking curve and are presented as an average of the two obtained values(Fig. 5 and 6).

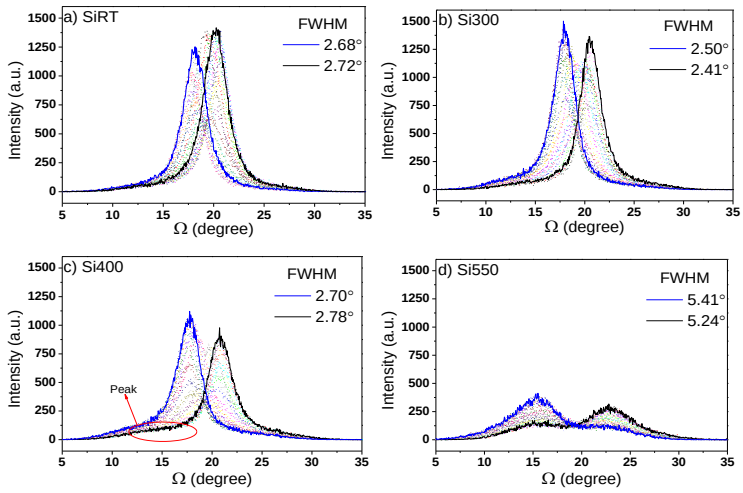

Fig. 5. The XRD rocking curve scans for different Φ-angles from 0 to 360° for (a) as-deposited and annealed 1 µm thick Al films deposited on Si substrate. The samples were annealed at temperatures of (b) 300 °C, (c) 400 °C and (d) 550 °C for 1 h in vacuum.

3.3.2. Rocking curves Si/Al

Fig. 5 shows the XRD rocking curves (ω-scans) of samples SiRT, Si300, Si400 and Si550 for all Φ values. The data of the figure gives a qualitative measure of the texture of the film. It is tied to the grain distribution (GD) of the (111) oriented grains in Al films. The data has been replotted in cylindrical coordinates which makes the visualization of the distribution easier as shown in Fig. 6. It shows that for SiRT (Fig. 6 (a)) the [111] directions of the Al grains have a small spread in tilt among the grains and the most frequent tilt of the Al [111] direction with the surface normal is around 1 degrees. In Fig. 5 the two ω-scans, drawn in solid lines (black and blue in color) are respectively the scan giving the largest peaks which have a rotation angle, Φ that is 180° with respect to each other. These scans give signal from the same grains and hence one could expect them to be mirror image of each other. The blue and black curves are qualitatively the mirror image of each other, but not quantitatively, which can be seen from difference in their peak intensity and FWHM. The crystal structure has mirror symmetry, but the shape of the grains and the grain boundaries which contribute to the peak by diffraction and scattering, do not have mirror symmetry. This is considered to be the reason for them being not perfectly mirror images in addition to possible instrumental misalignment. We see that the sample SiRT and Si300 shown in Fig. 6(a) and (b) respectively have one relatively narrow distribution of misalignments between the Al [111] directions. For higher annealing temperature as seen in Fig. 6(c) for Si400, there is also mainly one peak. However one can see small contributions from grains with larger misalignment. This is also seen from Fig. 5(c) as a small encircled shoulder corresponding to Al grains that have their [111] direction tilted about 3 degrees with respect to the surface normal. For even higher annealing temperature of 550 °C, as for Si550 shown in Fig. 5(d), the contribution from the larger tilts has increased significantly while the single peak for a tilt angle around one degree appears vanished. The texture shown in

Fig. 5(d) has roughly a conical shape with a half apex angle (tilt) around 3.2 degrees. The FWHM value of the rocking curve peak for as-deposited and annealed films up to 400°C was ~2.6°, while when annealing at 550 °C it increased to ~5.3°.

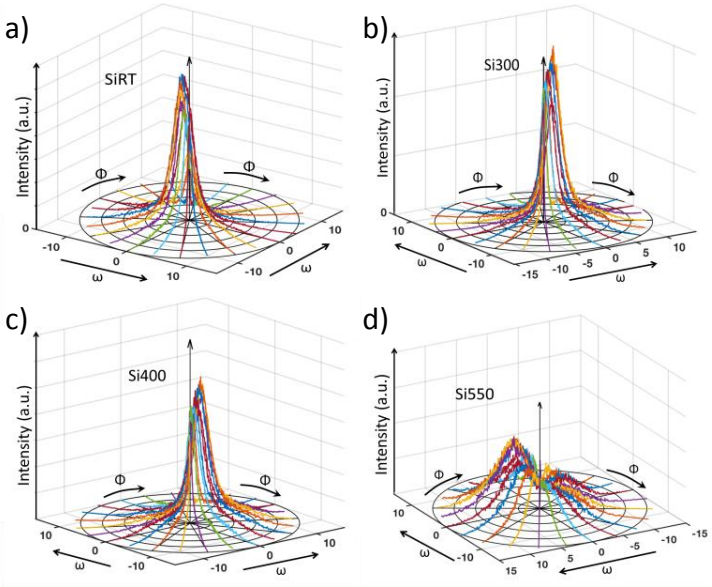

Fig. 6. The XRD rocking curve ω-scans as a function of rotation Φ angles for Si/Al samples annealed at different temperatures. It is the same data as in Fig. 5, plotted in cylindrical coordinates to visualize the grain distribution of (111) oriented grains. (a) as-deposited (b) annealed at 300 °C, (c) 400 °C, (d) 550 °C for 1 h . The 0° omega here is equivalent 19.2° omega in Fig.5.

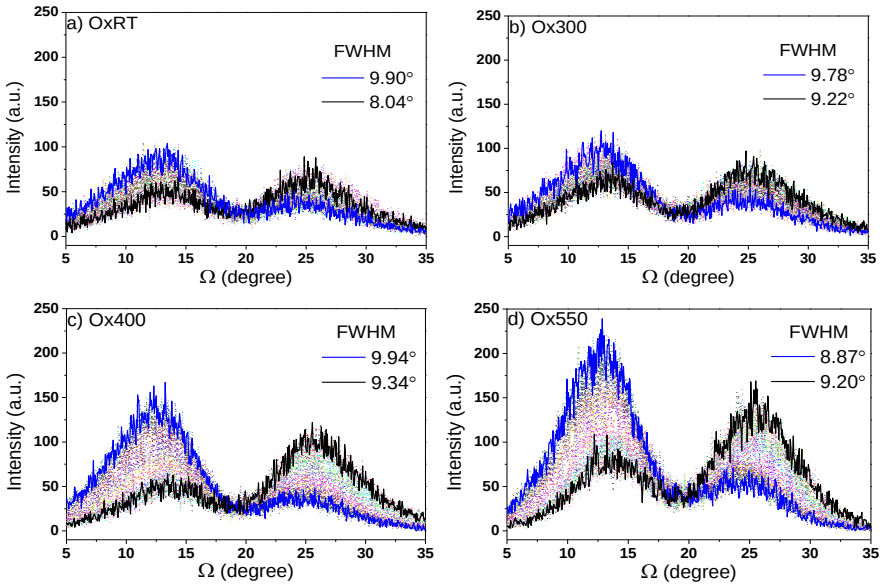

Fig. 7. The XRD rocking curve scans for different Φ-angles from 0 to 360° for (a) as-deposited and annealed 1 μm thick Al films deposited on oxidized Si having a 150 nm thick SiO_2 layer. The samples were annealed at temperatures of (b) 300 °C, (c) 400 °C and (d) 550 °C for 1 h in vacuum.

3.3.3. Rocking curves Si/ SiO_2/Al

Fig. 7 shows the raw XRD rocking curve scans of sample OxRT, Ox300, Ox400 and Ox550 while Fig. 8 displays the data in cylindrical coordinates. It is seen that the distribution of Al [111] orientations (see Fig. 8(a), OxRT) with respect to the surface normal is quite different for the as-deposited films on Si/SiO_2 than for those deposited on Si (see Fig. 6(a), SiRT). For OxRT the dominating tilt of the Al [111] direction with respect to the surface normal is around 6 degrees and this applies for all rotations (Φ). Thus the texture is essentially conical with a half apex angle of 6 degrees. The FWHM value for all samples was ~9°. On thermal annealing, the FWHM changed only by ±1° compared to its initial value of 9°. The intensity of the rocking curve peaks increased with an increase in annealing temperature. The peak intensities for the non-(111) orientations in Fig. 4 were too low to perform rocking curve measurements for these orientations.

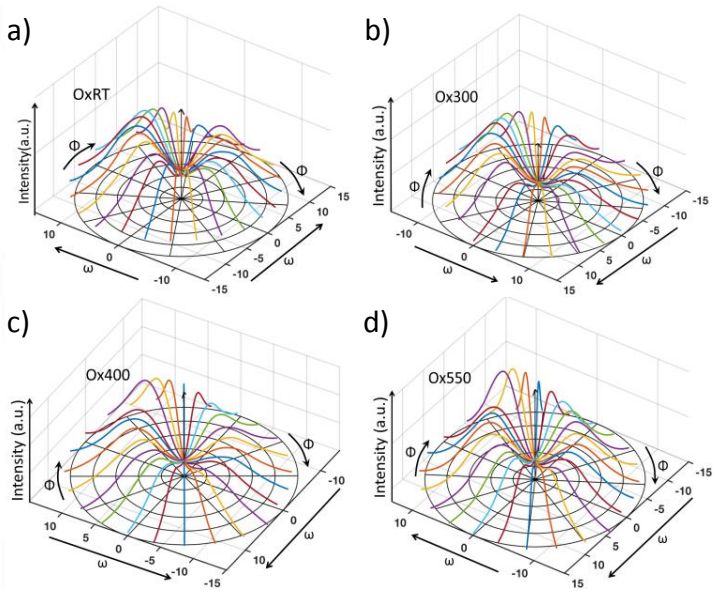

Fig. 8. The XRD rocking curve ω-scans as a function of rotation Φ angles for Si/SiO_2/Al samples annealed at different temperatures. It is the same data as in Fig. 7, plotted in cylindrical coordinates to visualize the grain distribution of (111) oriented grains. (a) as-deposited (b) annealed at 300 °C, (c) 400 °C, (d) 550 °C for 1 h. The 0° omega here is equivalent 19.2° omega in Fig.7.

3.3.4. Strain and grain size

The average (111) interplanar spacing for the grain around the maximum of the GD was determined by XRD, which yielded the corresponding strain. The resulting values for the strain in the film plane have been listed in Table 1. The strain values were tensile in the film plane and similar for different annealing temperatures for Si/Al and Si/SiO_2/Al samples.

The estimate of grain size from the Scherrer formula gave an average value between 164 and 177 nm. Considering that the films would likely contain dislocations, stacking faults, twins, micro stresses and grain boundaries, which would contribute to XRD peak broadening, and that

100-200 nm is considered to be a grain size so large that the Scherrer formula may not be applicable [30], it seems likely that the grain size is larger than the size estimated from the Scherrer formulae and hence these estimates will not be used further in the article.

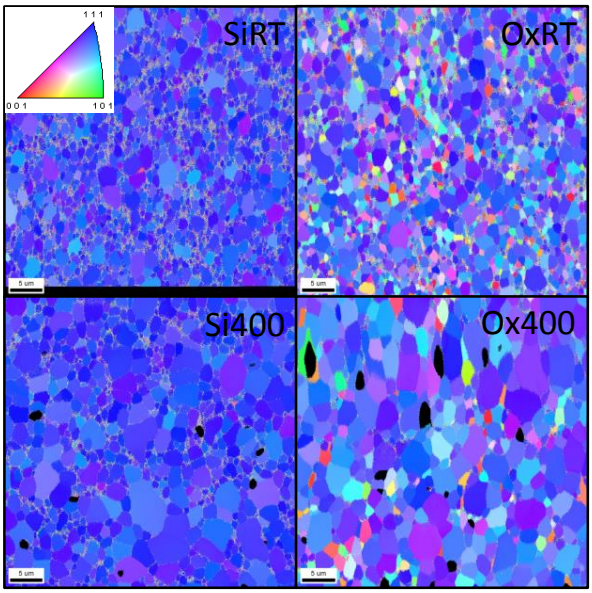

Fig. 9. Electron backscatter diffraction (EBSD) image for 1 µm thick Al films deposited directly on Si or deposited on oxidized Si having a 150 nm thick SiO_2 layer. The films were as-deposited and annealed at 400 °C. The legend on the top left shows the color coding of the film crystal/lattice orientation with respect to the SEM reference system (normal direction; perpendicular to the surface and parallel with electron beam, (TSL-OIM user manual v7.2, page 53) for different samples. Each colored area on the figure represents a grain of color coded orientation; separated from each other by grain boundaries. Black areas are non-indexed grains. The picture pixels represent the SEM electron beam displacement between each collected EBSD pattern.

3.4. EBSD results

3.4.1. Images of grains

EBSD images of samples SiRT, Si400, OxRT and Ox400 are shown in Fig. 9. The images in Fig. 9 represent the size and orientation of each single grain in an area of ~ 45 µm × 45 µm. The SiRT and Si400 samples had (111) as the preferred orientation. The samples OxRT and Ox400 showed (111) orientation for a large number of grains but other grain orientations were also clearly visible and spread all over the investigated area. One can clearly observe surface grain growth in both Si/Al and Si/SiO2/Al samples after annealing at 400 °C. In Fig. 9, a large number of small grains are visible at the grain boundaries for the as-deposited samples, but with annealing the small grains seem to have been engulfed by the bigger grains during the grain growth. In Fig. 9, the black regions are non-indexed regions. Most prominently, the SiRT sample exhibited more non-indexed regions than the OxRT sample. The non-indexed regions are regions with many grain boundaries giving no clear Kikuchi pattern. Interestingly, Si/Al samples exhibited these undefined features even after annealing up to 400 °C. In Fig. 9, images from only two samples are presented, but the other Si/Al and Si/SiO_2/Al samples which were annealed at

300 and 550 °C showed the same grain characteristics and trends except Ox550, which showed a preferred (111) orientation. The observed EBSD results on grain orientations are in good agreement the XRD analysis of Fig.4 regarding (111) preferred orientations.

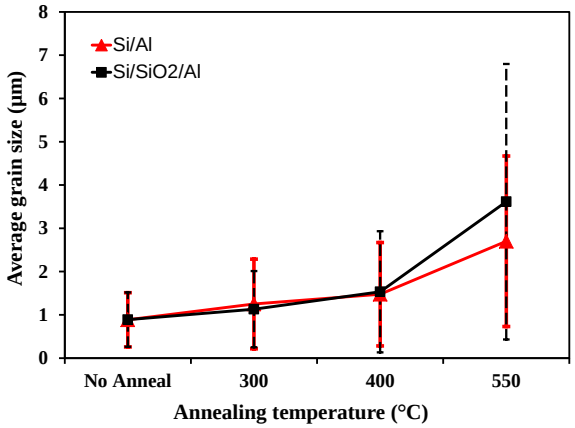

Fig. 10. The average grain size determined by analysis of EBSD scans of 1 µm thick Al films deposited on Si and deposited on oxidized Si having a 150 nm thick SiO_2 layer. The samples were annealed at 300, 400 and 550 °C for 1 h in vacuum. The error bars here represents the standard deviation in the grain size.

3.4.2. Grain size

The average surface grain size of Si/Al and Si/SiO_2/Al samples calculated from the EBSD images are presented in Fig. 10. The grain size of both Si/Al and Si/SiO_2/Al samples tended to increase with increasing annealing temperature. The average grain size for Si/Al and Si/SiO_2/Al samples increased from 0.9 µm at RT to 1.2 µm at 300 °C and 1.5 µm at 400 °C. The average grain sizes for Ox550 and Si550 were 3.6 µm and 2.7 µm, respectively. The differences in grain size were not statistically significant. However, the standard deviation of the grain size increased with increasing temperature, and was larger for Ox- than for Si-samples.

3.4.3. Inverse pole figures

The inverse pole figures (IPFs) of Si/Al samples obtained from EBSD data are shown in Fig.11. In these IPFs, orientations are plotted on a standard stereographic triangle with the crystallographic axes <001>,<101> and <111> for Al as the three corners. Each gridline inside the triangle represents 5°, hence the number of gridlines between the two crystallographic directions is a measure of the angle between those directions. For each sample there are two IPFs. The left hand side IPF shows the misorientation in degrees of each grain with respect to the [001] crystallographic direction of the Si substrate. Each point in Fig. 11 represents a grain in the EBSD image seen in Fig. 9. The [001] IPFs demonstrate a (111) preferred orientation of the Al film consistent with the XRD results. The spread in misorientation increased after annealing the sample at 550 °C.

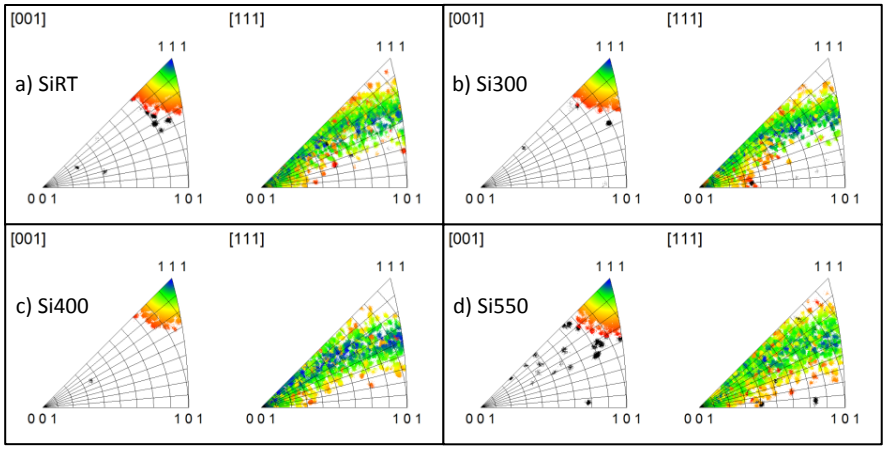

Fig. 11. The inverse pole figures extracted from EBSD data for (a) as-deposited and annealed 1 µm thick Al films deposited on Si substrate. The samples were annealed at temperatures of (b) 300 °C, (c) 400 °C and (d) 550 °C for 1 h in vacuum. For each sample the left diagram shows the orientation of the [001] crystallographic direction of the Si substrate relative to the crystallographic direction of the Al grains plotted on a standard stereographic triangle. The right diagram for each sample shows the same but for the [111] crystallographic direction of the Si substrate.

The right hand stereographic triangles of Fig.11 shows the orientation of the [111] direction of the Si substrate with respect to the crystallographic directions of the Al grains. It shows that the Al film has a <111> fiber texture. In a perfect <111> fiber texture the Al grains have their <111> crystallographic direction aligned with the surface normal while there are no preferred rotation angle for the grains around this axis. The theoretical [111] IPF for a perfect <111> texture is a curve starting at the [001] corner and ending up at 19.4 degrees away from the [111] corner towards the [101] corner. It can be seen that the dominating trend of the points in the [111] IPF follows such a line.

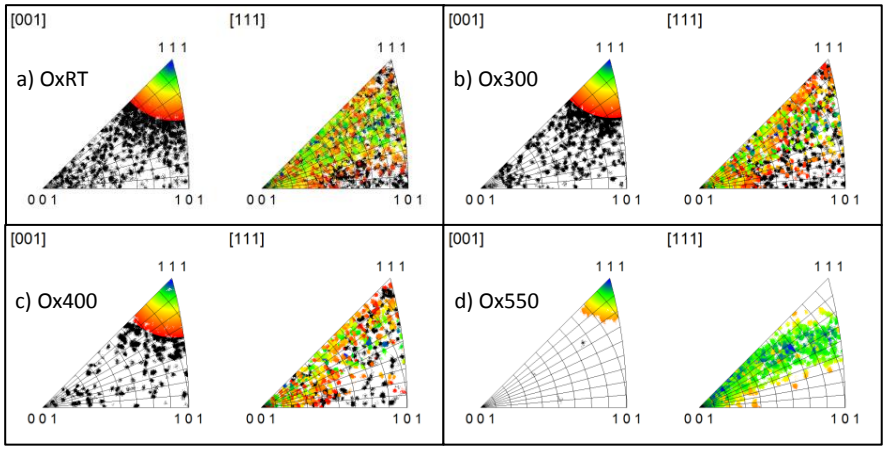

Fig. 12. The inverse pole figures extracted from EBSD data for (a) as-deposited and annealed 1 µm thick Al films deposited on Si/SiO_2 substrate. The samples were annealed at temperatures of (b) 300 °C, (c) 400 °C and (d) 550 °C for 1 h in vacuum. For each sample the left diagram shows the orientation of the [001] crystallographic direction of the Si substrate relative to the crystallographic direction of the Al grains plotted on a standard stereographic triangle. The right diagram for each sample shows the same but for the [111] crystallographic direction of the Si substrate.

Fig. 12 shows IPFs for the Si/SiO_2/Al samples. The misorientation for sample Ox25, Ox300, and Ox400 had a large spread in all directions. The misorientation was reduced for the higher annealing temperature of 500 °C. The IPFs indicate the presence of other crystallographic orientations than (111) in the OxRT, Ox300, and Ox400 samples, but a preferential (111) grain orientation in the Ox550 sample. This result is consistent with the XRD results (refer Fig. 4(inset)).

Si/Al	**SiRT**	**Si300**	**Si400**	**Si550**
SR (nm)	1.9	3.9	5.2	5.5
Orientation	(111)	(111)	(111)	(111)
Tilt* (degree)	1.6	1.2	1.3	2.7
FWHM tilt (degree)	2.7	2.5	2.8	5.3
Misorientation EBSD (degree)	10–15	10–15	10–15	10–15
Grain size EBSD (nm)	0.90	1.25	1.47	2.70
Si/SiO_2/Al	**OxRT**	**Ox300**	**Ox400**	**Ox550**
SR (nm)	3.3	6.2	7.4	8.0
Orientation	Mix	Mix	Mix	(111)
Tilt* (degree)	5.9	6.2	6.2	6.1
FWHM tilt (degree)	9	9.5	9.6	9.1
Misorientation EBSD (degree)	>15	>15	>15	10–12
Grain size EBSD (nm)	0.89	1.13	1.53	3.61

Table 2. Overview of measured structure and morphology parameters for as-deposited and annealed Si/Al and Si/SiO_2/Al samples at 300, 400 and 550 °C. Surface roughness (SR) was determined by AFM. Preferred orientation, tilt* of (111) oriented grains w.r.t. surface normal for the maximum in (111) GD and the FWHM value of this tilt was determined by XRD. The grain size and misorientation was obtained from EBSD.

3.5. Short summary of results

To summarize the most prominent structural characterization results, Table 2 lists some of the parameters that have been measured on the samples. Fig. 2 shows a modest difference in the surface roughness of the Si/Al and Si/SiO_2/Al samples. The roughness increased with annealing temperature. No hillocks were observed for any as-deposited samples, but occurred for all annealed samples. All samples showed a texture of preferred (111) orientation, however, also the presence of (100) and (110) (Fig. 4, 9) oriented grains was observed for the case of Si/SiO_2/Al

samples until annealing at 400 °C. The details of the GD for (111) oriented grains in the Al films were quite different for Si/Al (Fig. 6) and $Si/SiO_2/Al$ samples (Fig. 8). The as-deposited $Si/SiO_2/Al$ samples showed a conical texture (~6° half apex angle, 9° FWHM width). The Si/Al as-deposited sample on the other hand had a relatively sharp (111) GD (FWHM 2.7°) with a tilt at the maximum of (111) GD of 1.6° from the nominal surface normal. The EBSD results confirmed the XRD results and showed the presence of multiple orientations for $Si/SiO_2/Al$ samples. Grain sizes where around 1 um for both as-deposited sample type and increased with annealing temperature (Fig. 10).

4. Discussion

This section will be divided into two sub-sections. In the first section, 4.1, the observed Al thin film structure will be discussed in the light of previous reported works. In the second section, 4.2, the differences in structures of Al thin films and their probable influence on the bonding characteristics of Al thin films will be discussed.

4.1. Morphology of evaporated Al films

4.1.1. Preferred orientation and surface energy effects

The experimental observations clearly showed that both for Si/Al and $Si/SiO_2/Al$ samples the Al film had a texture dominated by (111) preferred orientation in the as-deposited cases and the annealed cases, though to varying degrees. This has been commonly observed for deposition of fcc metals including Al, and several texture features observed in this work are given in text books and review articles and are presented there as common for deposition of fcc metals [31, 32]. But as mentioned in the introduction, the degree of texture could not be exactly predicted and there are variations in the literature as to the exact temperature and degree of texture, amount of other orientations etc. Considering the strong dependence of microstructure on parameters that are not always documented or controlled (like partial pressure of oxygen and energy of arriving atoms), it seems natural that there is a spread in microstructure reported by different authors. On the other hand, the qualitatively similar behaviors suggest that our deposition seems free from artifacts or peculiarities and can be discussed as a typical fcc metal deposition. For the deposition temperatures and substrates used here we expect that the growth of the film during deposition was according to the Volmer-Weber growth mode where isolated islands were nucleated and grew until impingement forming grain boundaries. It has been reported that grain growth during the late stages of coalescence can lead to (111) texture for several fcc metals inclusive Al [32, 33]. The preferred orientation has been considered to come from a minimization of surface and interface energy. For fcc metals the (111) planes are the most densely packed planes and the (111) surface has the least density of frustrated bonds. Thus, grain growth being driven dominantly by surface energy minimization will lead to preferential growth of (111)-textured grains [32]. Kuznetsov et al. [34] estimated the surface energy for different Al surface orientations and reported that the surface energy values were ordered among the surfaces like: (111)<(100)<(110)

with magnitudes of $0.846<0.92<1.049$ J/m^2, respectively. This means that the densest plane, (111), has the lowest surface energy, and is the most preferred orientation for Al. Minimization of strain energy density could also influence the growth of different orientations [31].

4.1.2. Difference in texture of Si vs SiO_2

We have observed a difference in the texture of Si/Al and Si/SiO_2/Al in the as-deposited case as well as in their annealing behavior. These differences were mainly tied to the presence of other orientations than the (111), the wider GD of the (111) grains, and the larger tilt of the Al <111> directions with respect to the surface normal. The exact reasons for the difference are not clear. From the literature, the differences we observe may not be uniquely related to the different substrates as one can find reports overlapping our observations for either substrate. We thus expect that in our case for both Si/Al and Si/SiO_2/Al samples the Al film grew by similar mechanisms in the later part of the growth evolution with thickness. We expect the surface diffusion of Al on Si and on SiO_2 to be different, and that should have yielded a different concentration of critical nuclei, which again would have given a different Al film thickness for coalescence. The different diffusivities should come from the difference in interaction of Al atoms with the different substrates (Si vs SiO_2). The different substrates should also have initiated different preferred orientations of the islands formed until coalescence. Generally, the crystal orientation of islands has been reported to be random on amorphous substrates like SiO_2, while a single crystal surface would normally yield some preferred orientations. For the case of Al on Si epitaxial relationships between the Al film and Si have been reported [14, 21, 35, 36]. Note, however, that in the present case there are no indications of epitaxial relationships between the orientation of the complete 1 um thick film and the Si substrate. It was clearly seen from the interpretation of the IPF of sample SiRT (Fig. 11) for the <111> Si direction that there is no preferred Al orientation for the in-plane direction. This indicates that the strongest influence on the preferred orientation comes from surface and interface minimization after the coalescence process. The interface energy between Si/Al and SiO_2/Al would have been different during coalescence process for the different substrates.

4.1.3 Change in preferred orientation with annealing

Both the XRD and the EBSD results showed that the Si/SiO_2/Al films had (111), (200) and (220) orientations for annealing temperatures up to and including 400 °C (see Fig. 4 and 9). We observed a decrease in I(220)/I(111) ratio with increasing annealing temperature for the Si/SiO_2/Al samples and a transition to preferred (111) orientation in the Si/SiO_2/Al film when the annealing temperature was increased from 400 °C to 550 °C. In the review by Thompson [37], so-called ‘abnormal’ or ‘secondary grain growth’ is described to occur in films with columnar structures in which a few grains grow in size at the expense of the usually static matrix of normal grains. The abnormal grains generally have restricted crystallographic orientations which are a function of free surface energy of film surface and film/substrate interface. Hence, when

secondary grain growth occurs after deposition in fcc metal films deposited on an amorphous substrate, a strong (111) fiber texture will occur [37]. There is no clear evidence that there was a secondary grain growth during annealing of the present samples. There was a grain growth that required grain boundary movement. Some grains may have disappeared, such as the (200) and (220) grains for the $Si/SiO_2/Al$ sample. The disappearance may have occurred without nucleating new (111) grains. The signature of abnormal grain growth is a bimodal grain size distribution. We saw no clear evidence for that, except for the hillock formation and for sample Ox550 there were some grains that could be classified as abnormally large according to Thompson's definition.

4.1.4. Hillock formation

Fig. 3 shows higher density of hillocks in the $Si/SiO_2/Al$ than in the Si/Al films, and that the hillock density increased with increasing annealing temperature up to 400 °C, but that it decreased with increasing the annealing temperature further to 550 °C. Due the large thermal coefficient of expansion (TCE) mismatch between Si and Al, the Al film experiences a high compressive stress when the substrate is heated, that leads to hillocks formation. When the stress relaxation is non-uniform in the film, the material moves in the relaxed regions to reach equilibrium hence leading to the formation of hillocks [38]. Sanchez et al. reported that compressive stress gradients between (110) and (111) grains lead to hillock formation by abnormal growth of (110) grains out of the Al film plane [39]. As observed by XRD measurements (Fig. 4), (110) oriented grains were only observed in $Si/SiO_2/Al$ samples, except for the Ox550 sample which had a reduction in the area covered by hillocks. Martin et al. observed a correlation between increasing (111) film texture and decreasing hillock density [40]. This result on hillock density correlates well with the predominance of (111) grain orientation found by XRD measurements (see Fig. 4). Tensile stress in the film plane was present in both sample kinds and hillocks were also observed in both sample kinds. The occurrence of more hillocks in the $Si/SiO_2/Al$ samples could be due to the reasons stated above.

4.1.5. Rocking curves, comparison with literature

Queirolo et al. [24] found that an Al-Si film sputter deposited on oxidized Si substrate at room temperature gave a single peak in rocking curve analysis, which they interpreted as a uniaxial fiber texture. This is then similar to what we have observed for deposition of Al on a clean Si surface at room temperature. When Queirolo et al. made the deposition with a substrate temperature of 150 °C, they observed two peaks in the rocking curve and a low intensity (200) orientation peak occurred in the lock-coupled scan. They interpreted this as a cone shaped texture and a less pronounced preferential growth/orientation. This observation is similar to what we have observed for depositing Al on Si/SiO_2 at RT. We also have transformed the fiber texture observed for Si/Al to a cone shaped texture by annealing the film to 550 °C. This is included as an example that the structures we have observed could not be easily nor precisely predicted by

reports in the literature. Some of the variations making the prediction difficult can be that both atomic mobility and interface energies may depend upon impurities such as oxygen and this is not always well documented.

4.1.6. Rocking curves, comparison with EBSD and grain growth

The grain growth was clearly observed in our SEM/EBSD results. Grain growth by annealing indicates atomic mobility of Al atoms. Grain growth by annealing involves grain boundary motion, which again relies on inter-grain diffusion of Al. The increase in intensity of the rocking curve peaks for $Si/SiO_2/Al$ sample with increasing annealing temperature that we have observed (Fig. 7) is consistent with an increase in the areal density of the film having a specific orientation with respect to the surface normal, possibly combined with a decrease in the defects scattering of the X-rays due to grain growth. This is also consistent by the vanishing of non-(111) orientations in the XRD pattern of Fig. 4 (inset). Since the change in FWHM of the rocking curve peak was only $\pm$ 1°, we interpret the observations as a result of grain growth that mostly is due to grain boundary motion resulting in the disappearance of some grains. As mentioned in 4.1.1, abnormal grain growth is considered to give rise to a bimodal grain distribution in grain growth models [37]. The Ox550 sample did show a very wide distribution of grains and abnormal grain growth initiated at different stages or configuration could possibly have given that. In summary, the EBSD images show that Al grain growth, grain boundary motion, and Al-Al inter-grain diffusion has occurred in both $Si/SiO_2/Al$ and Si/Al samples at temperatures ranging from 300 to 550 °C. This is consistent with the rocking curves.

4.1.7. Grain size

As seen in Fig. 8, the average grain size on the sample surface found from EBSD measurements ranged from 1–3 μm, and increased with increasing annealing temperature. The grain size of our as-deposited Al films is similar to the grain size observed by Lita et al. [41]. Additional TEM results on the same films as reported here showed a grain size comparable to the Al film thickness, i.e. around 1 μm [42].

4.1.8. Tilt of [111] Al with respect to surface normal

The observation in rocking curves (Fig. 5 (d) and 7) of a texture where the dominating [111] axis of the Al grains makes a tilt angle (~6°) with the surface normal is interesting. This was observed for the as-deposited OxRT sample, for all annealed Ox samples, and for the sample Si550. In general, a (111) texture with a 0° tilt should be the result when minimization of surface energy and interface energy dominate the driving forces. While a tilt can be the result of strain energy minimization, it could also result from multiple twin structures and dislocations in the film [43]. Films with similar cone shaped texture to that we have observed have been reported by many different authors. For example, Gangulee and d'Heurle reported tilt angles of 8°–12° for Al-Cu films [44]. Longworth and Thompson found that the texture of their Al-alloy

films changed specifically from (111) to (112) [45]. A (112) texture does not fit our observations, however, a texture annotated as (997) by Kuhnke and Kern [46] could describe our situations. The surface for grains of (997) can consist of (111) terraces, 9 atoms wide divided by atomic step edges forming by a (111) microfacet. The surface belongs to classes of vicinal surfaces with (111) terraces. A fibrous texture for orientations like (445), (443), (997) and (779), could be described as a conical (111) texture where the tilt angle is 6.2, 7.3, 6.45 and 7° respectively, which are similar to the dominating tilt angles observed by rocking curves of samples mentioned above. Vicinal surfaces can play a large role in the growth of crystals, so also grains, while the energy and stability of such surfaces are currently considered for the possibility for nanoengineering of molecular structures on the surfaces [47].

4.2. Effect of Al thin film on wafer bonding differences

In the following, we will discuss how the currently observed differences in Al film morphology for Si/Al and Si/SiO_2/Al samples can be related to our earlier reported differences in bondability at lower temperatures (see Fig. 1). We recall that Fig. 1 shows Si/SiO_2/Al films have a higher bondability than Si/Al films. We usually expect that a high bondability for metal thermocompression bonding is accompanied by a high number of metal atoms on one surface making physical contact with atoms of the other surface to be bonded. For Al, direct contact between the metal atoms is prevented by a native oxide on Al. This oxide thus needs to be removed or broken. Both temperature and pressure will assist in that process.

4.2.1. Bonding at high temperature of 550 °C

At 550 °C the Si/SiO_2/Al and Si/Al films appeared to bond equally well. It is reasonable that the high and equal bondability at this high temperature was caused by plastic deformation of the Al film. The homologous temperature at 550 °C is: $T_H = T/T_m = 0.88$, where T_m is the melting temperature. At that high temperature the atomic mobility is high and Al softens, which leads to deformation and break down of the natural oxide followed by inter-diffusion and resulting in increased contact area between the bonding surfaces. The processes are thus in principle understood and the 500 °C case will not be discussed further. The correlations between film morphology and bondability will be discussed for the two film types for lower temperatures and the following will not apply to the 550 °C case.

4.2.2. Surface topography/roughness

Fig. 2 shows that there was a difference in surface roughness between the Si/Al and Si/SiO_2/Al films. Note that in our bonding process, the first contact between the Al film surfaces to be bonded occurred at room temperature. Therefore, the surface roughness of the samples OxRT and SiRT are relevant. Contact mechanics theory [48] and simulations [49] on elastic rough surfaces predict a decreasing bondability with increasing surface roughness. The same general predictions are made by several other contact mechanics theories mentioned in the

references, even if the details vary. The surface roughness was higher for the $Si/SiO_2/Al$ samples than for the Si/Al samples. Also, the areal density of hillocks on the $Si/SiO_2/Al$ samples was larger than that on the Si/Al samples. Therefore, the observations of higher bondability for $Si/SiO_2/Al$ than for Si/Al films (Fig. 1) cannot be explained by the surface roughness differences, according to the considerations of the mentioned theories.

On the other hand, it is not obvious what modifications would be made to the theoretical predictions by having a native oxide as in the present case. Intuitively, during the bonding process, the increase in contact area would progress differently before and after a local oxide fracture. For breaking of the oxide the asperity curvature should be important. It is a parameter that is related to the roughness and topology. One expects that a large curvature would ease the native oxide fracture by creating local high pressure points, whereas the bonding process after the oxide breaking would not have the same dependence on asperity curvature. We do not know the asperity curvature differences for our surfaces, but believe that the observed small difference of 1 nm in surface roughness between the $Si/SiO_2/Al$ and the Si/Al films is not giving rise to topologies that are responsible for the differences in bondability between $Si/SiO_2/Al$ and Si/Al films.

4.2.3. Al native oxide

The bondability could be affected by the dominant grain orientation through the Al_2O_3 formed on the Al thin film surface. Different phases of Al_2O_3 have been reported to form on different grain orientations. It has been reported that amorphous Al_2O_3 develops on Al with (100) and (110) orientation, while crystalline γ-Al_2O_3 develops on (111) Al [50]. However Billard et al. report that the air formed native Al_2O_3 is always amorphous [51]. It seems possible that differences in crystallinity of Al_2O_3 could impact the bondability of the mating Al films. The yield strength is expected to be different for the different phases. For several oxides the tensile strength is lower for the crystalline than for the amorphous phase, while for the compressive strength it is the other way around. For breaking the native oxide during bonding, it is considered that the shear strength of the oxide would be the most relevant parameter. Normally crystalline solids show a strong decrease in strength with temperature, while the strength of an amorphous material varies little with temperature because of the lack of slip planes [52]. Thus there are doubts whether there are different crystallinity oxides on the bonded samples and if there are, then the expected influence on the bondability of Si/Al vs. $Si/SiO_2/Al$ is opposite to the observed trend. Further, even if the oxides were different; the shear stress that will be exerted on the oxide layer should be largely dependent on the deformation properties of the Al and hence would not account for the observed differences in the bondablity at lower temperatures.

4.2.4. Diffusivities in Si/Al vs Si/SiO_2/Al

We have observed grain growth with increasing temperature, increase in surface roughness and growth of hillocks. These processes require self-diffusion in the Al film and local net transport of material. This increased Al diffusion with temperature could assist in merging the grains on opposing wafers during bonding, both by diffusion assisted creep of the asperities and filling in the voids by (surface) diffusion. If there was a difference in the amount of diffusion for Si/SiO_2/Al and Si/Al, that could contribute to the difference in bondability at lower temperatures. In the following, we consider surface diffusion, lattice/vacancy diffusion, and grain boundary diffusion.

T (°C)	**Surface diffusivity (D_s) (cm^2/s)**			**$\sqrt{D_s t}$ (μm) (time = 1h)**		
	(111)	**(100)**	**(110)**	**(111)**	**(100)**	**(110)**
25	2.0×10^{-6}	4.3×10^{-13}	1.6×10^{-14}	855	0.40	0.07
300	2.3×10^{-5}	3.2×10^{-8}	4.4×10^{-9}	2878	108	40
400	3.4×10^{-5}	1.9×10^{-7}	3.3×10^{-8}	3500	266	110
550	5.1×10^{-5}	1.4×10^{-6}	2.7×10^{-7}	4292	714	315

Table 3
Al surface diffusion coefficient (D_s) and the corresponding surface diffusion length ($\sqrt{D_s t}$) at (111), (100) and (110) oriented surfaces at temperatures of 25, 300, 400 and 550 °C for 1 h. The activation energy and the pre-exponential factor for surface diffusion of Al on Al for different orientations were taken from Agarwal et al. [53].

4.2.4.1. Surface diffusion

Theoretical self-diffusion studies by Agarwal et.al suggests that the self-diffusivities on the different surfaces of Al are very different and have very different activation energies [53]. We have used the diffusivity parameters in their publication to estimate the diffusivity and the diffusion length for 1 hour diffusion at our annealing temperatures. These estimates are given in Table 3 for Al on Al. The activation energy for Al diffusion on an Al (100) surface is four times larger than that on a (111) surface. At room temperature the characteristic diffusion length, $\sqrt{Dt}$, is 2000 times longer on the (111) surface than on the (100) surface and 12000 times longer than on the (110) surface. It can be anticipated that surface diffusion may play a significant effect in the bonding of two Al surfaces, in particular for the filling in of cavities between deformed asperities. Since the diffusion on the (111) oriented surface is faster compared to the other orientations, the maximum assistance to bonding can be expected by having (111) oriented Al surfaces. However, the surfaces of the Al grains in our bonding experiments were covered by a native oxide and the results from contamination free Al surfaces may not be directly applicable.

It can regardless be concluded that differences in surface diffusion created by differences in crystallographic orientations did not play a key role in the better bondability of Si/SiO_2/Al samples at lower temperatures compared to the Si/Al samples, since the mechanism would have favored the Si/Al samples which had only (111) preferred orientation.

4.2.4.2. Grain boundary and lattice-diffusion

Al can diffuse in Al along dislocations or along grain boundaries. Grain boundary diffusion in fcc metals plays an important role in transport of metal atoms. It provides an easy transport path for atoms and can dominate at low temperatures. Even at a homologous temperature of 0.5, the grain boundary diffusivity is ten orders of magnitude larger than lattice diffusion [54]. The mathematical treatment of grain boundary diffusion is based on a model first proposed by Fisher [55] and addresses the interdiffusion of different materials, but can describe self-diffusion by minor adjustments [56]. Self-diffusion by grain boundaries was analyzed by tracer diffusion. Radioactive atoms will spread by lattice diffusion, diffusion along grain boundaries and leaking of tracers from the grain boundary into the grains [56]. The processes can be unwound by fitting the radioactive depth profiles to theory. It is today common to follow Harrisons original classification [57] of the kinetics and the dominating processes. Depending upon the annealing times, grain size, lattice diffusivity and grain boundary parameters the kinetic follows an A, B or C type (corresponding to equations 1, 2 and 3 below). In type A kinetics the lattice diffusion dominates the transport, the lattice diffusivities are high, and the diffusion length is not very much larger than the spacing *d* between grain boundaries. In type B kinetics diffusion both by grain boundary and lattice contribute to the transport of tracers/material. Here, the lattice diffusion length is much smaller than the spacing between grain boundaries, *d*, which itself is considerably larger than the grain-boundary width. In type C kinetics, lattice diffusion is practically frozen and diffusion takes place along grain boundaries [57].

$$\sqrt{D_l t} \geq 1.25d, \tag{1}$$

$$s\delta \ll \sqrt{D_l t} \ll d, \tag{2}$$

$$\sqrt{D_l t} \ll s\delta. \tag{3}$$

In the above equations, D_l is the (lattice) diffusivity, t is the diffusion time, whereas, $\sqrt{D_l t}$ is the diffusion length. Further, d is the grain size, s is the segregation factor (1 for self-diffusion) and δ is the grain boundary width (order of interatomic distance ~0.5 nm).

Practical thin film diffusion usually obeys type B and or C kinetics. The diffusion coefficient and diffusion length during 1h ($\sqrt{D_i t}$) for lattice, dislocation pipe and grain boundary diffusion are calculated in Table 4 based on Al self-diffusion activation energy and pre-exponential factors obtained by data from Stechauner and Kozeschnik [58]. From Table 4, one can see that the diffusivity for grain boundary diffusion is much larger than that for dislocation diffusion and

lattice diffusion. The value of the characteristic diffusion length then follows the same order. To evaluate the significance of each process one would also have to consider a specific case and take into consideration the volume distribution of atoms contributing to the total volume displacement for each diffusion type. For our samples one can expect that diffusion follows: type A kinetics at and above 350 °C; type B kinetics in the temperature range of 300–350 °C; type C kinetics below 300 °C.

In order to relate the characteristic diffusion parameters of Table 4 to processes that are considered important for thermo-compression bonding, we can estimate how many Al atoms in the structure would have a large probability of diffusing to the top of the film and thus contribute to filling in a gap. Grain boundaries provide a pathway by which Al atoms can be transported to the surface and thereby could assist in filling in the voids between bonded regions at the interface. Lattice diffusion would also contribute to this. From the values in Table 4 and our measurements of grain sizes by EBSD (See Fig. 9) we can estimate how many atoms of Al can be transported in the structure by self-diffusion to a void per grain. For this simple estimate we can assume that grain boundary diffusion and lattice diffusion are independent. For grain boundary diffusion, the volume where Al atoms can be transported from to the surface is considered to be given by $\sim 4d\delta x_{gb}$, while for lattice diffusion it will be $d^2 x_l$. Using these formulae, it has been estimated that at 300 °C, grain boundaries can transport Al atoms which can fill up a volume up to 1.2 μm^3 per grain in an hour, while lattice diffusion can transport atoms filling a total volume of 0.5 μm^3 per grain. At 400 °C, $x_{gb} > 450 \times x_l$, but due to the small value of δ, the volume of atoms contributed by grain boundaries is half the size of that for lattice diffusion. These estimates of Al diffusion in an ideal Al structure also indicate that the diffusion should not be the factor that limits the bondability of Al-Al films around the bonding temperature of 300 °C if the transport is not hindered by something else other than the diffusivity in the ideal structure.

T(°C)	D_{gb} (cm^2/s)	D_{dp} (cm^2/s)	D_l (cm^2/s)	x_{gb}(μm)	x_{dp} (μm)	x_l (μm)
25	6.6×10^{-12}	4.3×10^{-17}	1.0×10^{-23}	1.5	4.0×10^{-3}	1.9×10^{-6}
300	7.0×10^{-7}	4.1×10^{-10}	4.2×10^{-13}	504	12	0.4
400	4.5×10^{-6}	5.4×10^{-9}	2.1×10^{-11}	1281	44	2.8
550	3.1×10^{-5}	8.1×10^{-8}	1.3×10^{-9}	3393	171	22

Table 4
Self-diffusion coefficients for Al grain boundary (D_{gb}), dislocation pipe (D_{dp}) and lattice (D_l) diffusion and the corresponding diffusion lengths ($x_i = \sqrt{D_i t}$) at temperatures of 25, 300, 400 and 550 °C for 1 h. The Arrhenius parameters for Al grain boundary, dislocation pipe and lattice diffusion were taken from Stechauner and Kozeschnik [58].

Taking into consideration the bonding parameters, there should be high enough diffusivity to achieve bonding for both sample types if there was no oxide on the Al surfaces acting as a diffusion barrier. Due to the presence of the Al native oxide on the Al surfaces, the diffusion of Al atoms across the bonding interface will be hindered. The diffusion kinetics also depends upon the diffusion temperature and grain size. For our two sample types (Si/Al and Si/SiO_2/Al) the grain size was similar at temperatures from RT to 400 °C and hence there should not be a considerable difference in the diffusion kinetics between the two sample types. Since the bondability was highly different for the two different sample types at these temperatures, the net transport of Al atoms that can be supplied by diffusion does not appear to be the single factor distinguishing the bondability of the Al films. We emphasize again that we are considering the difference in bondability. Diffusion kinetics is important for good bondability; it is just not the property that that can explain the large difference.

4.2.5. Effect of grain orientation on mechanical properties

It is likely that the difference in grain orientation of Si/Al and Si/SiO_2/Al samples caused the films to have different mechanical properties. Further, it is likely that these differences in mechanical properties contributed to the observed differences in the bondability of the films as we will explain and argue for in the following. During the bonding process the applied pressure and temperature can result in plastic deformation of Al films. This deformation can contribute to breaking of the native oxide, an increased contact interface between the opposing Al surfaces, and Al atom diffusion in and across the interface region, leading to the bonding between the Al films. Creep is one of the important mechanisms for plastic deformation. Creep depends upon the strength and duration of the applied stress, the temperature, and on the grain size and other material properties of the Al thin film. These factors will be further discussed in this section.

The applied stress in the experiments in Fig.1 was in the range from 68 MPa (when the applied force was distributed across the complete bonding surface) to very large (when only one or three asperities were touching at the beginning of the bonding process). The temperature regime, in Kelvins, for which creep is important in metals is considered to be $0.5T_m < T < T_m$. In the experiments in Fig.1 the applied temperature was in this range. Different creep mechanisms dominate depending on the value of σ/G, where σ is the applied stress and G is the shear modulus of the material [59]. During the bonding process, different number of points between the bonding surfaces will be in contact as the bonding will proceed. Due to differences in stress at the contact points, different creep mechanisms will dominate at different times during the bonding process because of change in contact area of surfaces.

It is well known that the yield stress for single crystal Al is dependent on the crystallographic orientation. The yield stress for single crystal Al (at room temperature) under uniaxial stress is much higher along the [111] direction than along other crystallographic directions (for example a factor 2 difference between [111] and [100]) [60]. This is related to a lower number of available {111}<110> slip systems for the configuration resulting from

applying the stress perpendicular to (111). A strong (111) texture may thus require a higher applied stress to facilitate plastic deformation than the stress required for random crystallographic orientations. The (111) orientation dominated for all our samples except the $Si/SiO_2/Al$ samples annealed at 400 °C and below.

The observed GD for (111) orientation in $Si/SiO_2/Al$ was much wider than that for Si/Al as determined from the XRD rocking curve analysis (not considering the 550 °C anneal case). The dislocations in the material can glide only under the effect of shear stress. According to the Schmid law, the metal flows plastically when the resolved shear stress acting in the plane and along the direction of slip reaches the critical value, τ_c. given by [59]:

$$\tau_c = \sigma_0 \sin\chi \cos\lambda \quad (4)$$

where, σ_0 is the normal stress applied to the specimen, χ is the angle between applied normal stress and slip plane, λ is the angle between applied normal stress and slip direction, $\sin\chi \cos\lambda = M$ and M is known as the Schmid factor.

The orientation for which fcc crystals are softest will have $M = 0.5$, which in our case has occurred approximately at the lower center of the IPF triangle with respect to [001] direction (see Fig. 11 and 12). The IPF diagram of $Si/SiO_2/Al$ samples showed a higher number of misoriented grains in the region where the value of M^{-1} will be 2 (except for anneal at 550 °C); while for Si/Al samples, misoriented grains lied in the region where the value of M^{-1} is in range of 3–3.5. Hence, more metal should flow plastically due to lower resolved shear stress in case of $Si/SiO_2/Al$ samples bonded at lower temperatures contributing to higher bondability compared to Si/Al samples. The dislocation densities in bonded $Si/SiO_2/Al$ samples at 400 °C were found to be higher compared to that in Si/Al as observed in the TEM study, which may have been due to aided plastic deformation due to lower value of resolved shear stress [42].

The nature of a grain boundary depends on the misorientation of the two adjoining grains and on the orientation of the boundary plane relative to them. Hence, depending on the misorientation angle, grain boundaries can be classified into three categories: low-angle boundaries, high-angle boundaries and special boundaries. Low-angle boundaries have a misorientation less than 15 degrees and high angle boundaries have a misorientation larger than 15 degrees. The trend is: the higher the misorientation angle, the higher is the grain boundary energy, the smaller is the gap between dislocations and the higher is the diffusion rate (except for special boundaries). Special boundaries are the high angle boundaries which have low energy due to the perfect fit of adjoining lattices. Examples of special boundaries are twin boundaries and coincidence site lattice, which corresponds to ~ 70.2° and 38.2° for {111} fcc metals. As seen in Fig. 11 and 12, $Si/SiO_2/Al$ samples had a higher degree of misorientation than Si/Al samples, especially at temperature of 400 °C and below. Although as discussed before, the grain boundary diffusion should have been almost similar for both samples but only for same angle boundaries with the same angle. Since high angle grain boundaries were observed in $Si/SiO_2/Al$

samples, they will have higher probability of fast diffusion of Al atoms through grain boundaries at lower temperatures.

4.2.6. Changing film morphology for obtaining higher bondability

Other deposition conditions than those we have used could give similar differences between $Si/SiO_2/Al$ and Si/Al films, or enhance the factors we have discussed and could be considered connected to an enhanced bondability at lower temperatures. For example, the structural features of multiple preferred directions in addition to (111) could be achieved in other ways than depositing on SiO_2 surface rather than Si. For example, depositing under increasing partial pressure of oxygen may increase the occurrence of other orientations. Also adding other elements to Al can have this effect. How these deposition processes would affect the bondability is unknown and would need to be found by experiments. The deposition procedures mentioned may however also have an effect on plasticity by interacting with dislocations, and can alter the glide of dislocations, thus the effect on bondability is uncertain. These approaches of engineering the microstructure of Al films can be a fruitful approach in labs and production lines where Al bonding is desired, but where removing the native oxide in the bonding machine just prior to bonding is not available.

5. Conclusions

The morphology of Al thin films deposited on Si with and without an SiO_2 layer have been studied by AFM, SEM, XRD, and EBSD; films were as-deposited or annealed at temperatures of 300, 400 and 550 °C for 1 h. The surface roughness and the number of hillocks on the Al film deposited on SiO_2 were higher than on the Al film deposited on Si. The XRD and EBSD results showed that the Al film deposited directly on Si only had (111) preferred orientation. The Al film deposited on SiO_2 consisted of grains with different orientations distributed all over the Al surface, except for the sample annealed at 550 °C, which had (111) oriented grains only. It was observed that Al films deposited on SiO_2 had conical <111> texture with a semi-apex angle of about 6°. For the Al film deposited on Si, a <111> fibrous texture was observed. No significant difference in the grain size of Al deposited on Si or SiO_2 could be observed except for samples annealed at 550 °C, where the Al film on SiO_2 had larger grain size than the Al film on Si. The measured differences in the morphology of Al thin films deposited on Si and SiO_2 are thought to account for earlier observed differences in the films bonding ability. Specifically, the presence of grain orientations other than (111) and the wider (111) GD of films on SiO_2 can influence the surface roughness, grain inter-diffusion, and plastic deformation and thereby also the break-up of a native aluminum oxide on the Al film. We have argued among the weight of these factors in enhancing the bondability of Al films, and have favored the plastic deformation as the most dominating reason for the observed enhanced bondability of Al films deposited on SiO_2 surfaces compared to Al films deposited on Si surfaces.

Acknowledgments

The authors wish to thank several colleagues for discussions on parts of this work, notably Dr. Patricia A. Carvalho from SINTEF, Prof. Bjørn Holmedal from NTNU, Øystein S. Fjellvåg and Heine N. Riise from UiO. Financial support from The Research Council of Norway through the project NBRIX (Contract No. 247781/O30) and MSENS (Contract No. 210601/O30) is gratefully acknowledged.

References

[1] R. Pelzer, H. Kirchberger, P. Kettner, Wafer-to-Wafer Bonding Techniques: From MEMS Packaging to IC Integration Applications, Electronic Packaging Technology, 2005 6th International Conference on, 2005, pp. 1-6.

[2] E. Masayoshi, Wafer level packaging of MEMS, Journal of Micromechanics and Microengineering 18(7) (2008) 073001.

[3] J. Froemel, M. Baum, M. Wiemer, F. Roscher, M. Haubold, C. Jia, T. Gessner, Investigations of thermocompression bonding with thin metal layers, Solid-State Sensors, Actuators and Microsystems Conference (TRANSDUCERS), 2011 16th International, 2011, pp. 990-993.

[4] S. Farrens, Metal based wafer level packaging, International Wafer-Level Packaging Conference, San Jose, CA 2008.

[5] M.M.V. Taklo, P. Storås, K. Schjølberg-Henriksen, H.K. Hasting, H. Jakobsen, Strong, high-yield and low-temperature thermocompression silicon wafer-level bonding with gold, Journal of Micromechanics and Microengineering 14(7) (2004) 884.

[6] A. Fan, A. Rahman, R. Reif, Copper Wafer Bonding, Electrochemical and Solid-State Letters 2(10) (1999) 534-536.

[7] V. Dragoi, G. Mittendorfer, J. Burggraf, M. Wimplinger, Metal Thermocompression Wafer Bonding for 3D Integration and MEMS Applications, ECS Transactions 33(4) (2010) 27-35.

[8] N. Malik, E. Poppe, K. Schjølberg-Henriksen, M.M.V. Taklo, T.G. Finstad, Environmental Stress Testing of Wafer-Level Al-Al Thermocompression Bonds: Strength and Hermeticity, ECS Journal of Solid State Science and Technology 4(7) (2015) P251-P257.

[9] N. Malik, K. Schjølberg-Henriksen, E. Poppe, M.M.V. Taklo, T.G. Finstad, AlAl thermocompression bonding for wafer-level MEMS sealing, Sensors and Actuators A: Physical 211 (2014) 115-120.

[10] C.H. Yun, J. Martin, L. Chen, T.J. Frey, Clean and Conductive Wafer Bonding for MEMS, ECS Transactions 16(8) (2008) 117-124.

[11] R. Fraux, J. Baron, STMicroelectronics' innovation in wafer-to-wafer bondingtechniques shrinks MEMS die size and cost !, 3D Packaging, i-Micronews Media, 2011, pp. 24-26.

[12] J. Martin, Wafer capping of MEMS with fab-friendly metals, 2007, pp. 64630M-64630M-6.

[13] N. Malik, K. Schjølberg-Henriksen, E. Poppe, M.M.V. Taklo, T.G. Finstad, Impact of SiO 2 on Al–Al thermocompression wafer bonding, Journal of Micromechanics and Microengineering 25(3) (2015) 035025.

[14] F.d. Heaurle, L. Berenbaum, Rosenberg, On the structure of aluminum films, Trans. Met. Soc. AIME 242 (1968) 502.

[15] J.J. Bellina, The effects of preadsorbed oxygen contaminant on the adsorption of Al on Si (111), Journal of Vacuum Science & Technology 11(6) (1974) 1133-1140.

[16] Y.H. Park, P. Roessle, E. Majewski, J.F. Smith, Electromigration in aluminum films prepared with a high rate magnetron sputtering cathode, Journal of Vacuum Science & Technology A 3(6) (1985) 2308-2311.

[17] D. Resnik, J. Kovač, M. Godec, D. Vrtačnik, M. Možek, S. Amon, The influence of target composition and thermal treatment on sputtered Al thin films on Si and SiO2 substrates, Microelectronic Engineering 96 (2012) 29-35.

[18] S. Vaidya, A.K. Sinha, Effect of texture and grain structure on electromigration in Al-0.5%Cu thin films, Thin Solid Films 75(3) (1981) 253-259.

[19] C.H. Choi, R.A. Harper, A.S. Yapsir, T.M. Lu, Epitaxial growth of Al(111)/Si(111) films using partially ionized beam deposition, Applied Physics Letters 51(24) (1987) 1992-1994.

[20] F.J. Lamelas, M.T. Tang, K. Evans-Lutterodt, P.H. Fuoss, W.L. Brown, Epitaxial orientations of aluminum on silicon (001), Physical Review B 46(23) (1992) 15570-15573.

[21] I. Yamada, H. Inokawa, T. Takagi, Epitaxial growth of Al on Si(111) and Si(100) by ionized-cluster beam, Journal of Applied Physics 56(10) (1984) 2746-2750.

[22] I. Petrov, P.B. Barna, L. Hultman, J.E. Greene, Microstructural evolution during film growth, Journal of Vacuum Science & Technology A 21(5) (2003) S117-S128.

[23] M. Dapor, G. Cicolini, F. Giacomozzi, M. Boscardin, G. Queirolo, Seeman-Bohlin X-ray diffraction study of Al-1 %Si thin films used in ULSI devices, Materials Letters 13(2–3) (1992) 142-146.

[24] G. Queirolo, M. Dellagiovanna, G. De Santi, Effect of the sputtering ambient contamination on the microstructure of Al–Si films, Journal of Vacuum Science & Technology A 7(3) (1989) 651-655.

[25] T. Lin, K.Y. Ahn, J.M.E. Harper, P.B. Madakson, P.M. Fryer, Relationship between substrate bias and microstructure in magnetron-sputtered Al ・ Cu films, Thin Solid Films 154(1 – 2) (1987) 81-89.

[26] www.imagemet.com).

[27] P. Scherrer, Bestimmung der Größe und der inneren Struktur von Kolloidteilchen mittels Röntgenstrahlen, Nachrichten von der Gesellschaft der Wissenschaften zu Göttingen, Mathematisch-Physikalische Klasse 1918 (1918).

[28] www.nordif.com.

[29] www.edax.com).

[30] A.K. Singh, Advanced X-ray Techniques in Research and Industry, IOS Press2005.

[31] C.V. Thompson, R. Carel, Grain Growth and Texture Evolution in Thin Films, Materials Science Forum 204-206 (1996) 83-98.

[32] C.V. Thompson, Structure evolution during processing of polycrystalline films, Annual Review of Materials Science 30 (2000) 159-190.

[33] S. Roberts, P.J. Dobson, The microstructure of aluminium thin films on amorphous SiO2, Thin Solid Films 135(1) (1986) 137-148.

[34] V.M. Kuznetsov, R.I. Kadyrov, G.E. Rudenskii, Calculation of Surface Energy of Metals and Alloys by theElectron Density Functional Method, J. Mater. Sci. Technol. 14(4) (1998) 320-322.

[35] F.K. Legoues, W. Krakow, P.S. Ho, Atomic structure of the epitaxial Al–Si interface, Philosophical Magazine A 53(6) (1986) 833-841.

[36] H. Niwa, M. Kato, Epitaxial growth of Al on Si(001) by sputtering, Applied Physics Letters 59(5) (1991) 543-545.

[37] C.V. Thompson, Grain growth in thin films, Annual Review of Materials Science 20 (1990) 245-268.

[38] P. Chaudhari, Hillock growth in thin films, Journal of Applied Physics 45(10) (1974) 4339-4346.

[39] J.E. Sanchez, E. Arzt, Effects of grain orientation on hillock formation and grain growth in aluminum films on silicon substrates, Scripta Metallurgica et Materialia 27(3) (1992) 285-290.

[40] B.C. Martin, C.J. Tracy, J.W. Mayer, L.E. Hendrickson, A comparative study of Hillock formation in aluminum films, Thin Solid Films 271(1–2) (1995) 64-68.

[41] A.E. Lita, J.E. Sanchez, Characterization of surface structure in sputtered Al films: Correlation to microstructure evolution, Journal of Applied Physics 85(2) (1999) 876-882.

[42] N. Malik, P.A. Carvalho, E. Poppe, T.G. Finstad, Interfacial characterization of Al-Al thermocompression bonds, Journal of Applied Physics 119(20) (2016) 205303.

[43] S. Mader, R. Feder, P. Chaudhari, Recrystallization of (001) oriented gold films into (111) orientation, Thin Solid Films 14(1) (1972) 63-78.

[44] A. Gangulee, F.M. D'Heurle, Anomalous large grains in alloyed aluminum thin films I. Secondary grain growth in aluminum-copper films, Thin Solid Films 12(2) (1972) 399-402.

[45] H.P. Longworth, C.V. Thompson, Abnormal grain growth in aluminum alloy thin films, Journal of Applied Physics 69(7) (1991) 3929-3940.

[46] K. Kuhnke, K. Kern, Vicinal metal surfaces as nanotemplates for the growth of low-dimensional structures, Journal of Physics: Condensed Matter 15(47) (2003) S3311.

[47] C. Didiot, S. Pons, B. Kierren, Y. Fagot-Revurat, D. Malterre, Nanopatterning the electronic properties of gold surfaces with self-organized superlattices of metallic nanostructures, Nat Nano 2(10) (2007) 617-621.

[48] L. Zhang, Y.-p. Zhao, Adhesion of rough surfaces with plastic deformation, Journal of Adhesion Science and Technology 18(6) (2004) 715-729.

[49] N. Mulakaluri, B.N.J. Persson, Adhesion between elastic solids with randomly rough surfaces: Comparison of analytical theory with molecular-dynamics simulations, EPL (Europhysics Letters) 96(6) (2011) 66003.

[50] L.P.H. Jeurgens, W.G. Sloof, F.D. Tichelaar, E.J. Mittemeijer, Thermodynamic stability of amorphous oxide films on metals: Application to aluminum oxide films on aluminum substrates, Physical Review B 62(7) (2000) 4707-4719.

[51] S. Billard, J.P. Fondère, B. Bacroix, G.F. Dirras, Macroscopic and microscopic aspects of the deformation and fracture mechanisms of ultrafine-grained aluminum processed by hot isostatic pressing, Acta Materialia 54(2) (2006) 411-421.

[52] D.H. Buckley, Surface effects in adhesion, friction, wear, and lubrication, Elsevier Science1981.

[53] P.M. Agrawal, B.M. Rice, D.L. Thompson, Predicting trends in rate parameters for self-diffusion on FCC metal surfaces, Surface Science 515(1) (2002) 21-35.

[54] A. Suzuki, Y. Mishin, Atomic mechanisms of grain boundary diffusion: Low versus high temperatures, Journal of Materials Science 40(12) (2005) 3155-3161.

[55] J.C. Fisher, Calculation of Diffusion Penetration Curves for Surface and Grain Boundary Diffusion, Journal of Applied Physics 22(1) (1951) 74-77.

[56] H. Mehrer, Grain-Boundary Diffusion, Diffusion in Solids: Fundamentals, Methods, Materials, Diffusion-Controlled Processes, Springer Berlin Heidelberg, Berlin, Heidelberg, 2007, pp. 553-582.

[57] L.G. Harrison, Influence of dislocations on diffusion kinetics in solids with particular reference to the alkali halides, Transactions of the Faraday Society 57(0) (1961) 1191-1199.

[58] G. Stechauner, E. Kozeschnik, Self-Diffusion in Grain Boundaries and Dislocation Pipes in Al, Fe, and Ni and Application to AlN Precipitation in Steel, Journal of Materials Engineering and Performance 23(5) (2014) 1576-1579.

[59] M.A. Meyers, K.K. Chawla, Mechanical Behavior of Materials, Cambridge University Press2009.

[60] U.F. Kocks, Polyslip in single crystals, Acta Metallurgica 8(6) (1960) 345-352.